Hierarchical network enabled flexible textile pressure sensors with ultra-high sensitivity, ultra-wide linearity and high-temperature resistance

Meiling Jia
Shenzhen Institutes of Advanced Technology, Chinese Academy of Sciences
Chenghan Yi
Shenzhen Institutes of Advanced Technology, Chinese Academy of Sciences
Yankun Han
Shenzhen Institutes of Advanced Technology, Chinese Academy of Sciences
Xin Li
Shenzhen Institutes of Advanced Technology, Chinese Academy of Sciences
Guoliang Xu
Shenzhen Institutes of Advanced Technology, Chinese Academy of Sciences
Ke He
Shenzhen Institutes of Advanced Technology, Chinese Academy of Sciences
Nianci Li
Shenzhen Institutes of Advanced Technology, Chinese Academy of Sciences
Yuxin Hou
Shenzhen Institutes of Advanced Technology, Chinese Academy of Sciences
Zhongguo Wang
Shenzhen Institutes of Advanced Technology, Chinese Academy of Sciences
Zhixun Wang
School of Electrical and Electronic Engineering, Nanyang Technological University, 50 Nanyang Avenue, 639798 https://orcid.org/0000-0001-9918-9939
Weimin Li
Shenzhen Institutes of Advanced Technology, Chinese Academy of Sciences
Wenjie Li
Shenzhen Institutes of Advanced Technology
Weiguo Su
National Key Laboratory of Science and Technology on Vessel Integrated Power System, Naval 16 University of Engineering
Lei Wei
School of Electrical and Electronic Engineering, Nanyang Technological University
https://orcid.org/0000-0003-0819-8325

Chunlei Yang
Chinese Academy of Sciences
Ming Chen (ming.chen2@siat.ac.cn)
Shenzhen Institutes of Advanced Technology, Chinese Academy of Sciences

Article

Keywords: pressure sensors, polyimide fabric, sensitivity, linearity range, high pressure, high temperature

Posted Date: July 2nd, 2021

DOI: https://doi.org/10.21203/rs.3.rs-633054/v1

Abstract

Thin, lightweight, and flexible textile pressure sensors with the ability to precisely detect the full range of faint pressure (< 100 Pa), low pressure (in the range of KPa) and high pressure (in the range of MPa) are in significant demand to meet the requirements for applications in daily activities and more meaningfully in some harsh environments, such as high temperature and high pressure. However, it is still a major challenge to fulfill these requirements simultaneously in a single pressure sensor. Herein, a high-performance pressure sensor enabled by polyimide fiber fabric with functionalized carbon-nanotube (PI/FCNT) is obtained *via* a facile electrophoretic deposition (EPD) approach. High-density FCNT is evenly wrapped and chemically bonded to the fiber surface during the EPD process, forming a conductive hierarchical fiber/FCNT matrix. Benefiting from the abundant yet firm contacting points, point-to-point contacting mode, and high elastic modulus of both PI and CNT, the proposed PI/FCNT pressure sensor exhibits ultra-high sensitivity (3.57 MPa^{-1}), ultra-wide linearity (3.24 MPa), exceptionally broad sensing range (~ 45 MPa), and long-term stability (> 4000 cycles). Furthermore, under a high working temperature of 200 ºC, the proposed sensor device still shows an ultra-high sensitivity of 2.64 MPa^{-1} within a wide linear range of 7.2 MPa, attributing to its intrinsic high-temperature-resistant properties of PI and CNT. Thanks to these merits, the proposed PI/FCNT(EPD) pressure sensor could serve as an E-skin device to monitor the human physiological information, precisely detect tiny and extremely high pressure, and can be integrated into an intelligent mechanical hand to detect the contact force under high-temperature (> 300 ºC), endowing it with high applicability in the fields of real-time health monitoring, intelligent robots, and harsh environments.

Introduction

Thin, flexible, and wearable pressure sensors have a great application perspective in electronic skins, healthcare monitors, soft robotics, artificial intelligence, et al[1–10]. To date, flexible pressure sensors are mainly divided into four types: capacitive, piezoelectric, triboelectric, and piezoresistive[11–20]. Among the proposed flexible pressure sensors, piezoresistive sensors are widely used owing to their low manufacturing cost, ease of fabrication as well as easy readout mechanism. Flexible piezoresistive pressure sensors are generally comprised of three parts: flexible matrix material (such as the frequently-used polydimethylsiloxane (PDMS), polyurethane (PU)), conductive materials (such as Au, Ag, Graphene, CNT), and electrode materials.

With the change of practical applications and customer needs, in addition to fulfilling the requirements of daily life (such as wearable healthcare monitoring at normal pressure and room temperature), there is an increasing demand for wearable pressure sensors that can be used in harsh environments, such as high temperatures and/or high pressures. For instance, real-time physiological monitoring of firefighters during the firefight action is extremely important to assess the level of danger and make a real-time and life-saving decision to protect firefighters. Besides, the real-time detection of pre-stresses (~ tens of MPa) within the composite sheath of high-speed permanent magnet motor rotor under high temperature (~ 200

^{0}C) is vital for the whole motor system, which requires a flexible yet thin pressure sensor with the applicability in both high-temperature and high-pressure condition. Thus, there is an urgent need to achieve a single pressure sensor that can precisely detect the full range of faint pressure (< 100 Pa), low-pressure (in the range of KPa, such as human motions), high pressure (in the range of MPa, for example, safety monitoring of road, rail, bridge, and tunnel) and can be used in harsh high-temperature and high-pressure environments. However, it is still a great challenge. Generally, high sensitivity is the basic requirement for realizing the detection of faint pressure, while the high modulus of the sensor material is an essential prerequisite to the broad sensing range. Here, the sensitivity $S=(\Delta I/I_0)/\Delta P$ is the ratio of the relative change in current or resistance with the applied pressure, which is mainly attributed to the variation of contact area (or structural change). In other words, the sensors' sensitivity S is proportional to the variation of the contact area. The linear range of the sensor mainly relies on the continuous yet equivalent variation of the contact area with the increasing pressure.

A typical method towards improving the sensitivity and linearity is to create nano-sized or micro-sized patterns on elastic polymer. For example, several PDMS geometrical features, including micro-pyramids, micro-hemispheres, and micro-semicylinders are demonstrated to be an effective method to improve the sensitivity and linearity[21–24]. In our previous work[25–28], we also show that the contacting modes play an important effect in the sensing performance and demonstrate that the point-to-point contacting mode is the optimum strategy. However, these elastic polymers are commonly subject to the disadvantage of low elastic modulus (10 KPa to 10 MPa) and low glass transition temperature, which reveals that the sensor response will saturate at low-pressure levels (namely narrow linearity range and sensing range), and the sensor is not suitable for the high-temperature environments. Besides, the fabrication of these micro/nano-structured elastic polymer/conductive layer often requires complex fabrication processes, such as UV lithography, ICP/RIE etching, E-beam evaporation/magnetron sputtering, et al. To address these issues, we adopt polyimide (PI) as the flexible matrix material, because PI possesses the merits of higher modulus and high-temperature-resistant properties compared to other elastic polymers[29–30] (Fig. 1a). However, high modulus usually leads to high stiffness. Namely, the deformation of PI under the external pressure is not large, which may result in low sensitivity and quick signal saturation. Therefore, creating a hierarchical network based on PI materials and the design of contact modes is essential. Chen et al. reported a wearable pressure sensor based on PI/CNT composite aerogels through the freeze-drying and thermal imidization process, showing a sensitivity of 11.28 KPa^{-1} in the linear range of 5 KPa and the sensing range of 61 KPa. The sensing mechanism can be attributed to the contact of the adjacent cell walls (surface contacts) upon external compression[31]. Jeong et al. proposed a flexible pressure sensor based on tip flattened micro-dome shaped PI film and CNT *via* conventional lithography, RIE etching, and lift-off process. The sensor presents a linear range of 50 KPa with a sensitivity of 5.66×10^{-3} KPa^{-1} and 3MPa sensing range[32]. However, these PI/CNT pressure sensors cannot fulfill the above-mentioned requirements, and there is a trade-off between sensitivity and linear-response range, which has hindered their practical applications to a large extent.

Herein, a facile and robust electrophoretic deposition (EPD) process is used to deposit functionalized carbon nanotubes (FCNTs) on PI fiber-based fabrics under an electric field. Within the PI fiber-based fabrics, plenty of micro- and nano-hierarchical pores built by the multilayer PI microfiber networks endow the matrix material with a large specific surface (more contacting points), high structural stability, and high flexibility (Fig. 1b). After the EPD process, the FCNTs are chemically bonded to the PI fiber surface, forming a conductive hierarchical network (Fig. 1b). Thanks to the abundant yet firm contacting points, point-to-point contacting mode (Fig. 1c), and high elastic modulus of both PI and CNT, we demonstrate a thin (~ 0.37 mm), lightweight (86.5 mg/cm^3), flexible and wearable pressure sensor that is able to detect pressures from below 100 Pa all the way up to 45 MPa, which corresponds to the range from faint pressure (the weight of an aluminum particle) to low pressure (joint movement) to very high pressure (the weight of an automobile) with ultrahigh sensitivity (3.57 MPa^{-1} within a wide linear range of 3.24 MPa). Furthermore, thanks to the intrinsic temperature resistance of both PI and CNT, the proposed sensor also can detect the pressure up to 40 MPa and exhibit an ultrahigh sensitivity of 2.64 MPa^{-1} within a wide linear range of 7.2 MPa at 200 ºC and can work at higher temperatures above 300 ºC, indicating its high applicability in harsh high-temperature and high-pressure environments (Fig. 1d).

Results And Discussion

In order to obtain a uniform and conductive hierarchical network based on PI fiber/CNT structure, we designed and fabricated four sets of pressure sensors, namely PI/CNT(Stirring), PI/FCNT(Stirring), PI/CNT(EPD), and PI/FCNT(EPD). First, we used the conventional mechanical stirring method to incorporate CNT into the PI fiber fabric (Fig. 1e, PI/CNT(Stirring)). As shown on the right session of Fig. 1e, we can clearly see that only part of the PI fiber fabric turns black while other regions remain unchanged. The underlying reason for this non-uniformity is due to the agglomeration behavior of CNT during the stirring process[33], as confirmed in Fig. 1f-1h. Furthermore, these agglomerated CNT tend to be gathered in the gaps of the PI fibers rather than the PI surface (Fig. 1f-1h, Figure S1a). To improve the uniformity, a highly acidic and thermal oxidation process was used as the initial step to modify the CNT. This process not only was beneficial to the wettability and dispersibility of the CNT, but also made the CNT functionalized with negatively charged carboxyl group[34]. An EPD process was then adopted to deposit FCNT on PI fiber fabric (Fig. 1i). Under an electric field, these FCNTs migrated to the PI fiber fabric (anode) and evenly wrapped to the fiber surface (Figure S2a), as evidenced by the optical and SEM images of PI/CNT(EPD) (Fig. 1j-1l). It is worth noting that benefiting from the high-porous PI fiber fabric structure, these FCNTs would migrate to each fiber and be uniformly coated onto the fiber surface, even for the fibers adhered to the anode (Figure S2b). Figure S1b and Figure S3a represent the doping mechanism and the morphology of PI/FCNT(Stirring) and PI/CNT(EPD), respectively. Compared to PI/CNT(Stirring), FCNT is relatively evenly distributed on the PI fiber surface for PI/FCNT(Stirring), however, the coverage degree is still far below that of PI/FCNT(EPD). The least effective doping method is the EPD process with CNT, and we only observed a thin layer of CNTs adhered to one surface (away from the anode) of the PI fiber fabric (Figure S3b). This is well understood because CNT cannot move directionally to the PI fibers under an applied electric field. In general, the optical and SEM morphology

images show that the best strategy for obtaining a uniform and conductive network is through adopting the modified CNT with the EPD process. Conceivably, compared to the other three kinds of pressure sensors, the abundant contacting points within the conductive hierarchical network will be very beneficial to enhance the sensitivity, sensing range, and reliability of the PI/FCNT(EPD) pressure sensor.

The above results indicate that the modified CNT plays an important role in the proposed PI/FCNT(EPD) pressure sensor. To further probe into the intrinsic reason, we explored the interaction between PI fiber and FCNT, physical properties and structure difference between FCNT and CNT by transmission electron microscopy (TEM), Raman spectroscopy, Fourier transform infrared (FTIR) spectroscopy, and X-ray photoelectron spectroscopy (XPS). Figure 2a-c and 2d-f are the TEM images of CNT and FCNT, respectively. The tube diameter is decreased from ~ 16 nm for CNT to ~ 8 nm for FCNT, which is helpful to improve the dispersion. This partly accounts for the better uniformity for PI/FCNT(Stirring) compared with PI/CNT(Stirring). Raman spectra of CNT and FCNT are shown in Fig. 2g. Two characteristic peaks, located at 1321 cm^{-1} (D band) and 1587 cm^{-1} (G band), are observed for CNT. After modification, it shows a similar Raman spectrum (D band and G band) but with a more distinguishable D^+ band and narrower full-width at half maximum (FWHM). This is because the modification process improves the structural order and purity of the CNT[35–36]. Here, the D and D^+ bands represent a double-resonance Raman mode, which is due to the amorphous carbon, disorder, defects, or ion intercalation between the graphitic walls. The G band is due to the tangential in-plane stretching vibrations of the carbon-carbon bonds within the graphene sheets.

FTIR spectroscopy analysis of the FCNT provides the direct evidence of the successful modification with CNT (Fig. 2h and 2i), showing the characteristic band at 1536, 1573, and 1730 cm^{-1} which are due to C = O stretching vibration within the carboxyl and carbonyl functional groups[36]. Note that these characteristic peaks are not observed in CNT. Other notable peaks such as 1386 and 1634 cm^{-1} observed in both CNT and FCNT are ascribed to the C-O and O-H stretching vibration, respectively.

The existence of strong chemical interactions between FCNT and PI can be deduced from the Raman spectra, XPS, and FTIR analysis, as shown in Fig. 2j-l. As for the Raman spectra shown in Fig. 2j, two characteristic peaks of PI at 1377 and 1620 cm^{-1} are observed, corresponding to the stretch vibration of C-N within the imide ring and the aromatic imide ring vibrations of the dianhydride portion (green line). It is interesting to note that from the PI/FCNT(EPD) Raman spectra (red line) we can find that two prominent peaks, located at 1335 and 1605 cm^{-1}, are the overlap and broadening of the characteristic peaks of PI and FCNT, which is mainly attributed to the charge transfer between PI and FCNT[31,37–38]. The XPS spectra in Figure S4 show the characteristic peaks of both PI and PI/FCNT(EPD) centered at C1s (285.2 eV), N1s(400 eV), and O1s(532 eV). Compared with PI, the PI/FCNT(EPD) demonstrates an increment of C1s and O1s peak intensity and decrement of N1s peak intensity, which is owing to the existence of FCNT. Furthermore, as depicted in Fig. 2k for the C1s spectrum, we observe that there is a decreased intensity of the C = C/C-C, C-N, and C-O for PI/FCNT(EPD) compared to that of the PI, which again shows the existence of chemical interactions between FCNT and PI[34]. We further performed FTIR

analysis of PI and PI/FCNT (EPD), as displayed in Fig. 2l. Several notable absorption peaks located at 1370, 1499, 1714, and 1776 cm^{-1} are clearly observed for PI, which are caused by C-N, C = C stretching vibration, C = O symmetric, and asymmetric stretching, respectively. For PI/FCNT, these absorption peaks shifted to a low wavenumber direction, and the intensity is significantly reduced which is due to the strong interaction between PI and FCNT. And these strong chemical interactions come from the created strong hydrogen bonds between C = O and C = N of imide ring and carboxyl groups of FCNT[31,37–38]. In a word, the best doping effect that emerged in PI/FCNT (EPD) is attributed to the directional migration of FCNT during the EPD process as well as the formed strong hydrogen bonds between PI and FCNT.

Next, we consider the sensing performance of the proposed four sets of pressure sensors. To better understand the sensing mechanism for the PI fiber/CNT architectures and compare their sensing performance, we adopted Creo/Engineering to build the PI fiber/CNT model and finite element modeling (FEM) to analyze the dynamic working process of the pressure sensors under external pressure. Figure S5a-c shows the established models for PI/CNT(stirring), PI/FCNT(stirring), and PI/FCNT(EPD), respectively. Note that the PI/CNT(EPD) pressure sensor is not taken into consideration, because there is only a thin layer of CNT adhered to one surface of the PI fiber fabric (Figure S3b) and the conductive network is not formed. According to the SEM results shown in Fig. 1, Figures S1-S2, the established conductive contact mode for PI/CNT(stirring), PI/FCNT(stirring) and PI/FCNT(EPD) is CNT cluster to CNT cluster, CNT cluster to PI/FCNT fibers, PI/FCNT fibers to PI/FCNT fibers (Figure S5a-c), respectively. Dynamic microscopic deformation processes for these models are displayed in Figs. 3a-c and Figures S6-S8. Figure 3d shows the contacting area as a function of time for the four sets of pressure sensors. As the time increases from 0 to 1s, the increment speed of the number contacting for PI/FCNT(EPD) is far above that of the other three types of pressure sensors, indicating that the PI/FCNT(EPD) pressure sensor possesses the highest sensitivity. Besides, the contacting area gradually increases without saturation as the external pressure exceeding 2 MPa, revealing a broad working range for the proposed PI/FCNT(EPD) pressure sensor. The theoretical results presented in Fig. 3d and 3e agree well with the experimental results as detailed below.

To experimentally evaluate the performance of the proposed pressure sensors, we set up an intelligent data-acquisition device containing a universal electric signal analyzer Keithley 2400 and a computer-controlled dynamic positioning system. The effects of the CNT morphology and doping technique on the sensitivity of the proposed pressure sensors were studied by measuring the output current change as a function of applied external pressure, as shown in Fig. 4a-b. The size of all the pressure sensors is 5 mm (length) × 5 mm (width) × 0.37 mm (thickness). As we expected, the PI/FCNT(EPD) pressure sensor exhibits much higher current change under the same external pressure (namely, much higher sensitivity) and broader sensing range than that of other sets of pressure sensors, showing an excellent agreement with the theoretical prediction (Fig. 3). PI/FCNT(EPD) pressure sensor exhibits an ultrahigh sensitivity of 3.57 MPa^{-1} with an outstanding linearity up to an applied pressure of ~ 3.24 MPa and an exceptionally broad sensing range up to 45 MPa. The performances of the recently reported high-performance pressure sensors are summarized in Fig. 4c where the linearity range is the horizontal axis, and the sensitivity is

the vertical axis[31,32,39–45]. Excellent comprehensive properties including ultra-high sensitivity, ultra-broad linearity range and sensing range are found in the proposed PI/FCNT(EPD) pressure sensor. We attribute this excellent performance to the abundant yet firm contacting sites (high-density FCNT is evenly wrapped and chemically bonded to the PI fibers *via* EPD process), point-to-point contacting mode within the hierarchical conductive network, and high elastic modulus of both PI and CNT.

Our proposed PI/FCNT(EPD) pressure sensor not only can work at high pressure but also can operate at high temperatures. Figure S9 are the infrared (IR) thermal imaging images of the PI/FCNT(EPD) pressure sensor placed on a heat source, respectively. It can be seen that even if the heating temperature exceeds 300 ºC, the morphology and the temperature distribution of the PI/FCNT(EPD) pressure sensor almost remains the same during a heating period of 5 min. We also characterized its sensing performance at 200 ºC (see Methods), as depicts in Fig. 4b. The proposed sensor device still exhibits an ultrahigh sensitivity of 2.64 MPa^{-1} within a wide linear range of 7.2 MPa. Note that because the conductance of CNT is increased with the temperature, in the initial stage, the sensitivity of the pressure sensor reaches ~ 4.71MPa^{-1} within the linear range of 1.04 MPa at 200 ºC, which is higher than that at room temperature. Then the sensitivity decreased and was finally stabilized (Figure S10), and the measured sensitivity (2.64 MPa^{-1}) may due to the fact that some residual triethylamine molecules absorbed on the PI molecular chain are released, resulting in a slight decrease in weight (loss of some contacting sites), which is also verified by the thermogravimetric analysis, as shown in Figure S11. Furthermore, it is found that the weight loss for PI/FCNT(EPD) is higher than that of CNT. This is due to the excellent thermal conductivity of CNT, which serves as a heating source to induce the decomposition of PI. It is worth mentioning that although the thermal stability is decreased for PI/FCNT(EPD) fabric, the $T_{5\%}$ (the temperatures at 5% weight loss) still exceeds 350 ºC. Overall, these high-temperature experimental results demonstrated the flame retardancy and good heat stability of the proposed PI/FCNT pressure sensors, enabling their potential to be used in harsh high-temperature conditions.

Besides the sensitivity and sensing range, another electric characteristic of the PI/FCNT(EPD) pressure sensors was also tested. Figure 4d is the current-voltage (I-V) curves of the PI/FCNT(EPD) under various applied pressures. The I-V curves exhibit high linearity, revealing its excellent ohmic performance independent of the applied voltage. Figure 4e represents the current response of the PI/FCNT(EPD) pressure sensor over five on/off cycles under various external pressures (1.1 MPa, 1.3 MPa, 1.6 MPa, 2 MPa, and 7 MPa). The current experienced fast-changing under the repeated pressure loading and relaxation cycles. Besides, the current remained unchanged during the pressure loading process, indicating the robust repeatability and excellent reliability of the PI/FCNT(EPD) pressure sensors independent of the applied pressures. We further explored the sensors' durability by repeated loading and unloading pressure of 1.1 MPa for more than 4000 cycles, as shown in Fig. 4f. It is found that the sensor maintained its function with minimal output signal degradation. This excellent endurance behavior can be attributed to the strong chemical interaction between PI and FCNT as well as the good compressibility of both PI fiber fabric and CNT. In addition, the fabricated sensor exhibits a fast rise time of 100 ms and a relaxation time of 80 ms (Fig. 4g), which also indicates that the force unloading process is faster than

that of the loading process. The response time is mainly determined by the elastic recovery of the PI fiber fabric. Finally, the electric characteristics including I-V linearity and reliability of the sensor under 100 ^{o}C were also tested. As shown in Fig. 4h-i, the results demonstrate high linearity and excellent reliability of the PI/FCNT(EPD) pressure sensor, further endowing it with high applicability in high-temperature environments.

These sensing characterizations and analyses demonstrate that the proposed PI/FCNT(EPD) pressure sensor exhibits excellent sensing performance including ultra-high sensitivity, ultra-wide linearity, exceptionally broad sensing range, and high-temperature-resistant properties. The ultra-high sensitivity and ultra-wide linearity reveal that the resulting sensor can act as an ideal candidate to precisely detect the faint pressure (< 100 Pa), low-pressure (in the range of KPa, such as human motions), and high pressure (in the range of MPa). To testify the sensing capability, we conducted the following experiments and further explored their applications in real life. First of all, as shown in Fig. 5a, we put a small meter screw (0.161 g, ~ 63.1 Pa) on the sensor. The corresponding current change is displayed in Fig. 5b (red line), which shows that such a tiny pressure change can be precisely detected. Moreover, the limit of detection of our sensor device was also measured to be ~ 8.2 Pa, as depicted in Fig. 5b (blue line, an aluminium particle, 0.021 g). Secondly, we explored the sensor's ability as a skin-mountable human motion detector. For the test, the fabricated PI/FCNT(EPD) pressure sensor was attached to various parts of the human body, as shown in Fig. 5c-f. As a result, the fabricated PI/FCNT(EPD) pressure sensor is highly responsive to the repetitive dynamic flexion and straightening motions of the finger joint, wrist, elbow, and ankle. Besides, the cycling tests show that the response and relaxation behaviors are reproducible. The above results clearly suggest that the human motions can be identified with the PI/FCNT(EPD) pressure sensor, enabling its potential to serve as an E-skin device to monitor human physiological information in real-time.

To further improve the practicability of the PI/FCNT(EPD) pressure sensors, a real-time, wireless pressure monitoring system is developed, including data acquisition, wireless data transmission, and display *via* APP interface on a mobile phone, as displayed in Fig. 5g. Here, the function of the processing unit shown in Fig. 5g involves the data acquisition collected from the pressure sensor, analog-digital conversion, and wireless data transmission. With the real-time pressure monitoring system, we carried out two high-pressure experiments: (1) the PI/FCNT(EPD) pressure sensors was first compressed to a reference high-pressure of 15.8 MPa, followed by adding a metal with weighing about ~ 3.8 Kg, which is equivalent to a pressure increment of 1.5 MPa. The real-time pressure monitoring during the metal loading and unloading process is displayed by the APP interface, as shown on the right session of Fig. 5g. The results show that the PI/FCNT(EPD) pressure sensor can detect relatively small changes in pressure under extremely high pressures, even though the sensor is in a non-linear state (as shown in Fig. 4b). This significantly extends its available pressure sensing range, demonstrating its high potential use in the real-time precise detection of extremely high pressure. (2) Another experiment is the pressure detection of a vehicle during the running process (Fig. 5h). The PI/FCNT(EPD) pressure sensor is repeatedly rolled by the front wheel of a car. The recorded real-time pressure data is collected from APP and displayed in

Fig. 5i. When the car is driven over the sensor, the pressure increases instantaneously and comes back to its original state without any noticeable time lag. Besides, the sensor remained its function after the repeated rolling process. This greatly enables its application in the industry, such as safety monitoring of road, rail, bridge, and tunnel.

An ideal intelligent robot should not only require the basic capability of sensing force and pressure, but also can collect some characteristic data in some harsh high-temperature conditions (for example, firefighting). As a proof of concept, we designed the following experiments. We wrapped the PI/FCNT(EPD) pressure sensor in the fingertips of a mechanical hand while the mechanical hand is mounted on a computer-controlled stepping motor. The mechanic hand with the conformally wrapped sensor moved forward to a high-temperature object (> 300 ºC). When the sensor device touched the surface of the hot object, the output current increased. Here, we set a threshold current for the stepping motor. The stepping motor stopped and moved backward when the output current of the sensor device reached the threshold current. Figure 5j and 5k show the IR images as the mechanic hand moved close to and touched the hot object, respectively. The temperature of the fingertip increased from the room temperature to 81.5 ºC and 249 ºC, respectively. Figure 5l shows the current responding curve of the PI/CNT(EPD) pressure sensor during the “close, touch, feel and response” process. We observe that the current rises steeply to the threshold value and recovers quickly, demonstrating its great potential to serve as a wearable and high sensitivity pressure sensor that is able to withstand harsh environment where high temperature is present.

Discussion

This study demonstrates that the PI/FCNT(EPD) flexible textile pressure sensor is very promising and able to detect ultra-wide range pressure with high sensitivity, even for high temperatures (> 300 ºC). These merits endow it with high applicability in many applications. The future scope for this study is to carry out extensive work on further exploring the sensor’s P-I performance under different high temperatures. To keep the P-I curves unchanged during the whole heating process, adopting the composite conductive materials (for example, FCNT + metal nanoparticles) which include both negative and positive temperature coefficient of resistance (TCR) materials would address this issue. Furthermore, although the current application of the fabricated PI/FCNT(EPD) sensors focuses on the daily activities and harsh high temperature and high-pressure condition, these thin, lightweight, flexible textile pressure sensors and the corresponding wireless pressure sensing system are ready to be used in practical biomedical applications, because they are resistant to most chemical attacks.

Conclusion

In conclusion, we have developed a simple, robust, and effective method *via* modification process and EPD method for fabricating high-performance wearable pressure sensors. High-density FCNT is evenly wrapped and chemically bonded to the PI fibers *via* the EPD process. Benefiting from these abundant yet firm contacting points, point-to-point contacting mode within the hierarchical conductive network and

high elastic modulus of both PI and CNT, the proposed PI/FCNT pressure sensor possesses the merits of a thin thickness (~ 0.37 mm), lightweight (86.5 mg/cm^3), ultra-high sensitivity (3.57 MPa^{-1}), ultra-wide linearity (3.24 MPa) and exceptionally broad sensing range (~ 45 MPa). Furthermore, thanks to the high-temperature-resistant properties of both PI and CNT, the PI/FCNT pressure sensor device still exhibits an ultrahigh sensitivity of 2.64 MPa^{-1} within a wide linear range of 7.2 MPa. Besides, we have developed a real-time, wireless pressure monitoring system and demonstrated that the pressure sensor could serve as an E-skin device to monitor the human physiological information, precisely detect extremely high pressure, and can be integrated into an intelligent mechanical hand to detect the contact force under the harsh high-temperature environment.

Methods

Fabrication of PI/FCNT(EPD) Piezoresistive Pressure Sensor. FCNT was obtained by the modification process of CNT. CNT was purchased from XFNANO Co., Ltd. Next, 1.044g CNTs were dispersed in 40 ml of the mixture of concentrated sulphuric acid (30 ml) and concentrated nitric acid (10 ml) in a flask. The mixture was then stirred using a magnetic stirrer at 150°C for 1 h. The resulting dispersion was then diluted in water, and filtered repeatedly until the solution PH = 7, followed by the drying process in vacuum at 40°C overnight. The detailed fabrication process of PI fiber fabric and PI films can be found in our previous work[46]. Functional carbon nanotube dispersions were used to electrophoretically deposit nanotubes onto the PI fiber fabric. 0.1046g FCNT was dispersed in 100 ml anhydrous alcohol and then stirred using magnetic for 7 h. The PI fiber fabric was placed in contact with a stainless steel cathode as the anode. The same stainless steel was placed a fixed distance from the anode. EDP process was carried out under direct current with the voltage of 30 V for 1 h. The PI/FCNT fiber fabric was then dried in an oven for 10 min at 60°C. After the EPD and process, the PI/FCNT fiber fabric was cut into the designed concave shape, as shown in Fig. 1a and 1c. The active area is 5 mm × 5 mm,, the thickness is 0.37 mm, as shown in Figure S12. Cu wire electrodes are adhered to the bulgy area of the sensor through the conductive silver paste.

Fabrication of PI/CNT (Stirring), PI/FCNT(Stirring), and PI/CNT(EPD) Piezoresistive Pressure Sensor. PI/CNT (Stirring) pressure sensor: 0.1046g CNT was dispersed in 100 ml anhydrous alcohol. Then the PI fiber fabric is immersed in the CNT dispersion and stirred using a magnetic stirrer for 7 h. The subsequent baking and tailoring process is the same as PI/FCNT (EPD). PI/FCNT (Stirring): Compared with the PI/CNT (Stirring) pressure sensor, besides the difference of the functional layer (FCNT instead of CNT), the other process is the same. PI/CNT (EPD): Compared with the PI/FCNT (EPD) pressure sensor, besides the difference of the functional layer (CNT instead of FCNT), the other process is the same.

Encapsulation, characterization, test, and simulation. Two PI film is placed on and under the pressure sensor, respectively, forming a sandwich structure. Then this sandwich structure is further encapsulated by the PI adhesive tape. The morphologies of the PI fiber fabric and PI/FCNT(EPD) are characterized using SEM (AEISS SUPRA55). The morphologies of CNT and FCNT are further characterized using TEM (JEM-3200FS). Raman analysis was carried out on a Witec CRM200 backscattering Raman system. For

XPS measurement, ESCALAB 250Xi was used. For FTIR measurement, Frontier was used. TGA analysis was conducted on a thermogravimetric analyzer (Mettler Toledo, Switzerland) from room temperature to 800 ^{O}C. A semiconductor parameter analyzer Keithley 2400 was employed to measure the current – time (I – t) characteristics of the pressure sensors. The cycling performance of the pressure sensor was determined using a pressure meter (Dongguan Zhiqu Precision Instrument Co., Ltd). Oscilloscope (LUCK-3, digital storage oscilloscope, Chengdu Rongte Instrument Co., Ltd.) was used to measure the response and recovery time. In order to theoretically study the sensing performance of the pressure sensors, Creo and Ansys software were employed in the simulation. We first design and built the PI/CNT models via Creo software, then the established models were imported into Ansys software for further analysis. The PI fiber was modeled as a homogeneous isotropic elastic material with Young's modulus E = 2.5 GPa, and Poisson's ratio v = 0.34. For high temperature (100 and 200 ºC) P-I and other electric characterization, the PI/FCNT(EPD) pressure sensor was heated along with the metal supporting stage from room temperature to 100(200) ºC until the temperature of both the metal supporting stage and PI/FCNT (EDP) reach the steady state. Considering the change of CNT conductance and some residual triethylamine molecules absorbed on the PI molecular chain may be released under high temperature, the P-I performance of the PI/FCNT(EPD) pressure was characterized every ten minutes until obtaining a stable P-I curve.

Declarations

NOTE

The authors declare no competing financial interest.

Author Contributions

Jia, C. Yi and Y. Han contributed equally to this work.

ACKNOWLEDGMENTS

This work was partially supported by the Shenzhen Basic Research Grant: JCYJ20200109114801744, JCYJ20180507182431967, JCYJ20180507182445460,the National Nature Science Foundation of China (11804354, 61774164, 51903249). This work was supported in part by the Singapore Ministry of Education Academic Research Fund Tier 2 (MOE2019-T2-2-127), the Singapore Ministry of Education Academic Research Fund Tier 1 (MOE2019-T1-001-103 and MOE2019-T1-001-111) and the Singapore National Research Foundation Competitive Research Program (NRF-CRP18-2017-02). This work was also supported in part by Nanyang Technological University.

References

1. Kim, J. et al. Soft wearable pressure sensors for beat-to-beat blood pressure monitoring. Adv. Healthc. Mater. 8, e1900109 (2019).
2. Schwartz, G. et al. Flexible polymer transistors with high pressure sensitivity for application in electronic skin and health monitoring. Nat. Commun. 4, 1859 (2013).
3. Boutry, C. M. et al. A sensitive and biodegradable pressure sensor array for cardiovascular monitoring. Adv. Mater. 27, 6954(2015).
4. Tang, X, Wu, C, Gan, L, et al. Multilevel Microstructured Flexible Pressure Sensors with Ultrahigh Sensitivity and Ultrawide Pressure Range for Versatile Electronic Skins. Small, 2019, 15(10): e1804559.
5. Rus, D. & Tolley, M. T. Design, fabrication and control of soft robots. Nature 521, 467 (2015).
6. Liu, M. Pu, X. Jiang, C. et al. Large-Area All-Textile Pressure Sensors for Monitoring Human Motion and Physiological Signals. Adv Mater, 2017, 29(41).
7. Wang, X. Dong, L. Zhang, H. et al. Recent Progress in Electronic Skin. Adv Sci, 2015, 2(10): 1500169.
8. Wang, X. Gu, Y. Xiong, Z. et al. Silk-molded flexible, ultrasensitive, and highly stable electronic skin for monitoring human physiological signals. Adv Mater, 2014, 26(9): 1336–42.
9. Zhu, B. Ling, Y. Yap, L, W. et al. Hierarchically Structured Vertical Gold Nanowire Array-Based Wearable Pressure Sensors for Wireless Health Monitoring. ACS Appl. Mater. Interfaces 2019, 11, 29014–29021.
10. Meng, K. et al. A wireless textile-based sensor system for self-powered personalized health care. Matter 2, 896 (2020).
11. Peng, X. et al. A breathable, biodegradable, antibacterial, and self-powered electronic skin based on all-nanofiber triboelectric nanogenerators. Sci. Adv. 6, eaba9624 (2020).
12. Lin, L. et al. Triboelectric active sensor array for self-powered static and dynamic pressure detection and tactile imaging. ACS Nano 7, 8266–8274(2013)
13. Chen, J. et al. Soft robots with self-powered configurational sensing. Nano Energy. 77, 105171(2020)
14. Bai, N. et al. Graded intrafillable architecture-based iontronic pressure sensor with ultra-broad-range high sensitivity. Nat. Commun. 11, 209 (2020).
15. Luo, Y. et al. Flexible capacitive pressure sensor enhanced by tilted micropillar arrays. ACS Appl Mater. Interfaces 11, 17796–17803 (2019).
16. Huang Y, Fan X, Chen S C, et al. Emerging Technologies of Flexible Pressure Sensors: Materials, Modeling, Devices, and Manufacturing. Advanced Functional Materials, 2019, 29(12).
17. Yang Y, Pan H, Xie G, et al. Flexible piezoelectric pressure sensor based on polydopamine-modified BaTiO3/PVDF composite film for human motion monitoring. Sensors and Actuators A: Physical, 2020, 301.
18. Ma Y, Liu N, Li L, et al. A highly flexible and sensitive piezoresistive sensor based on MXene with greatly changed interlayer distances. Nat Commun, 2017, 8(1): 1207.

19. Luo C, Liu N, Zhang H, et al. A new approach for ultrahigh-performance piezoresistive sensor based on wrinkled PPy film with electrospun PVA nanowires as spacer. Nano Energy, 2017, 41: 527–534.
20. Gao L, Zhu C, Li L, et al. All Paper-Based Flexible and Wearable Piezoresistive Pressure Sensor. ACS Appl Mater Interfaces, 2019, 11(28): 25034–25042.
21. Zhu, B. et al. Microstructured Grapheme Arrays for Highly Sensitive Flexible Tactile Sensors. Small 2014, 10, 3625–3631.
22. Peng, S. et al. Rational Design of Ultrasensitive Pressure Sensors by Tailoring Micorscopic Features. Adv. Mater. Interfaces 2018, 5, 1800403.
23. Wang, Z. et al. Highly Sensitivity, Wearable, Piezoresistive Pressure Sensors Based on Irregrlar Microhump Structures and its Applications in Body Motion Sensing. Small 2016, 12, 3827–3836.
24. Jian, M. et al. Flexible and highly sensitive pressure sensors based on bionic hierarchical structures. Adv. Funct. Mater. 2017, 27, 1606066.
25. He, K, et al. High-performance zero-standby-power-consumption-under-bending pressure sensors for artificial reflex arc. Nano Energy 2020, 73, 104743.
26. Chen, M. et al. Touchpoint-Tailored Ultrasensitive Piezoresistive Pressure Sensors with a Broad Dynamic Response Range and Low Detection Limit. ACS Applied Materials & Interfaces 2019, 11 (2), 2551–2558.
27. Yi, C. et al. Highly Sensitive and Wide Linear-Response Pressure Sensors Featuring Zero Standby Power Consumption under Bending Conditions. ACS Applied Materials & Interfaces 2020, 12 (17), 19563–19571.
28. Li, W. et al. Flexible and High Performance Piezoresistive Pressure Sensors Based on Hierarchical Flower-Shaped $SnSe_2$ Nanoplates. ACS Applied Energy Materials 2019, 2 (4), 2803–2809.
29. Liaw, D. et al. Advanced Polyimide Materials: Syntheses, Physical Properties and Applications. Prog. Polym. Sci. 2012, 37, 907–974.
30. Gouzman, I. et al. Advances in Polyimide-Based Materials for Space Applications. Adv. Mater. 2019, 31, No. e1807738.
31. Chen, X. et al. Highly Compressible and Robust Polyimide/Carbon Nanotube Composite Aerogel for High-Performance Wearable Pressure Sensor. ACS Applied Materials & Interfaces 2020, 11, 42594–42606.
32. Jeong, Y. et al. Ultra-Wide Range Pressure Sensor Based on a Microstructured Conductive Nanocomposite for Wearable Workout Monitoring. Advanced Healthcare Materials 2021,10, 2001461.
33. Vaisman, L. et al. The role of surfactants in dispersion of carbon nanotubes. Adv Colloid Interface Sci, 2006, 128–130: 37–46.
34. Hilding J, Grulke E A, George Zhang Z, et al. Dispersion of Carbon Nanotubes in Liquids. Journal of Dispersion Science and Technology, 2007, 24(1): 1–41.

35. Niu F, Guo R, Dang L, et al. Coral-like PEDOT Nanotube Arrays on Carbon Fibers as High-Rate Flexible Supercapacitor Electrodes. ACS Applied Energy Materials, 2020, 3(8): 7794–7803.
36. Osswald S, et al. Monitoring oxidation of multiwalled carbon nanotubes by Raman spectroscopy. Journal of Raman Spectroscopy, 2007, 38(6): 728–736.
37. Qin Y, Peng Q, Ding Y, et al. Lightweight, superelastic, and mechanically flexible graphene/polyimide nanocomposite foam for strain sensor application. ACS nano, 2015, 9(9): 8933–8941.
38. Ramakrishnan, S., et al. "Synthesis and characterization of graphene oxide–polyimide nanofiber composites." RSC Advances 4.19 (2014): 9743–9749.
39. Li, H., et al. "Ultrahigh-Sensitivity Piezoresistive Pressure Sensors for Detection of Tiny Pressure."ACS Applied Materials & Interfaces 2018, 10, 20826–20834.
40. Li, X., et al. "Ultracomfortable Hierarchical Nanonetwork for Highly Sensitive Pressure Sensor."ACS Nano 2020, 14, 9605–9612.
41. Guan, X., et al. "Flexible Piezoresistive Sensors with Wide-Range Pressure Measurements Based on a Graded Nest-like Architecture." ACS Applied Materials & Interfaces 2020, 12, 26137–26144.
42. Li, Z., et al. "A wide linearity range and high sensitivity flexible pressure sensor with hierarchical microstructures via laser marking." Journal of Materials Chemistry C 2020, 8, 3088.
43. Lee, Y., et al. "Flexible Ferroelectric Sensors with Ultrahigh Pressure Sensitivity and Linear Response over Exceptionally Broad Pressure Range."ACS Nano 2018, 12, 4045–4054.
44. Zhu, M., et al. "Hollow MXene Sphere/Reduced Graphene Aerogel Composites for Piezoresistive Sensor with Ultra-High Sensitivity."Advanced electronic materials 2020, 6, 1901064.
45. Pang, Y., et al. "Flexible, Highly Sensitive, and Wearable Pressure and Strain Sensors with Graphene Porous Network Structure." ACS Applied Materials & Interfaces 2016, 8, 26458–26462.
46. Ma, P. et al. Investigate of Mo films deposited on high temperature polyimide substrate by magnetron sputtering for flexible CIGS thin film solar cells applications. AIP advances 2019, 9, 045024.

Figures

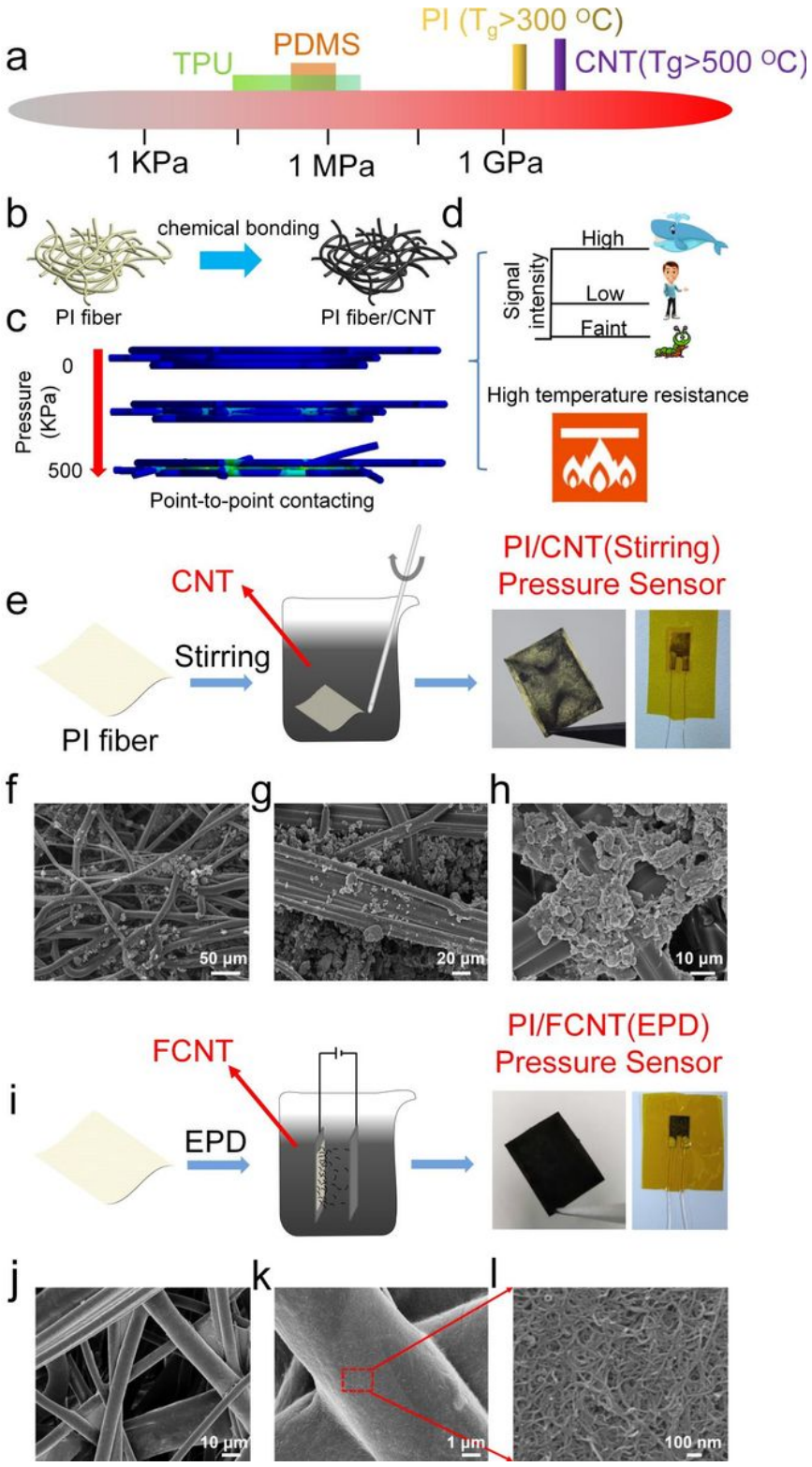

Figure 1

Materials selection, structure optimization, sensing mechanism and the fabricated PI/CNT(Stirring), PI/FCNT(EPD) pressure sensors. (a) Materials selection: schematic illustration of Young's modulus of frequently used flexible matrix materials and conductive materials for the pressure sensors. (b) Structure optimization: PI fiber-based fabrics, which containing plenty of micro- and nano-hierarchical pores, is adopted as the flexible matrix materials. Compared with PI film or PI aerogel, more contacting points

variation is expected within this structure. CNT is adopted as the conductive materials. (c) Sensing mechanism: contacting points variation of the PI fiber fabrics/CNT under external pressure from 0-500 KPa. (d) Schematic illustration of the response of the proposed PI fiber fabrics/CNT pressure sensor to faint, low, and high pressure, and such proposed pressure sensor possesses the merit of high-temperature resistance. (e) Schematic illustration of the fabrication process of PI/CNT(Stirring) fabric, optical images of the PI/CNT(Stirring) fabric, and the final encapsulated PI/CNT(Stirring) pressure sensor. (f-h) Top-view SEM images of the PI/CNT(Stirring) fabric. (i) Schematic illustration of the fabrication process of PI/FCNT(EPD) fabric, optical images of the PI/FCNT(EPD) fabric, and the final encapsulated PI/FCNT(EPD) pressure sensor. (j-l) Top-view SEM images of PI/FCNT(EPD) fabric.

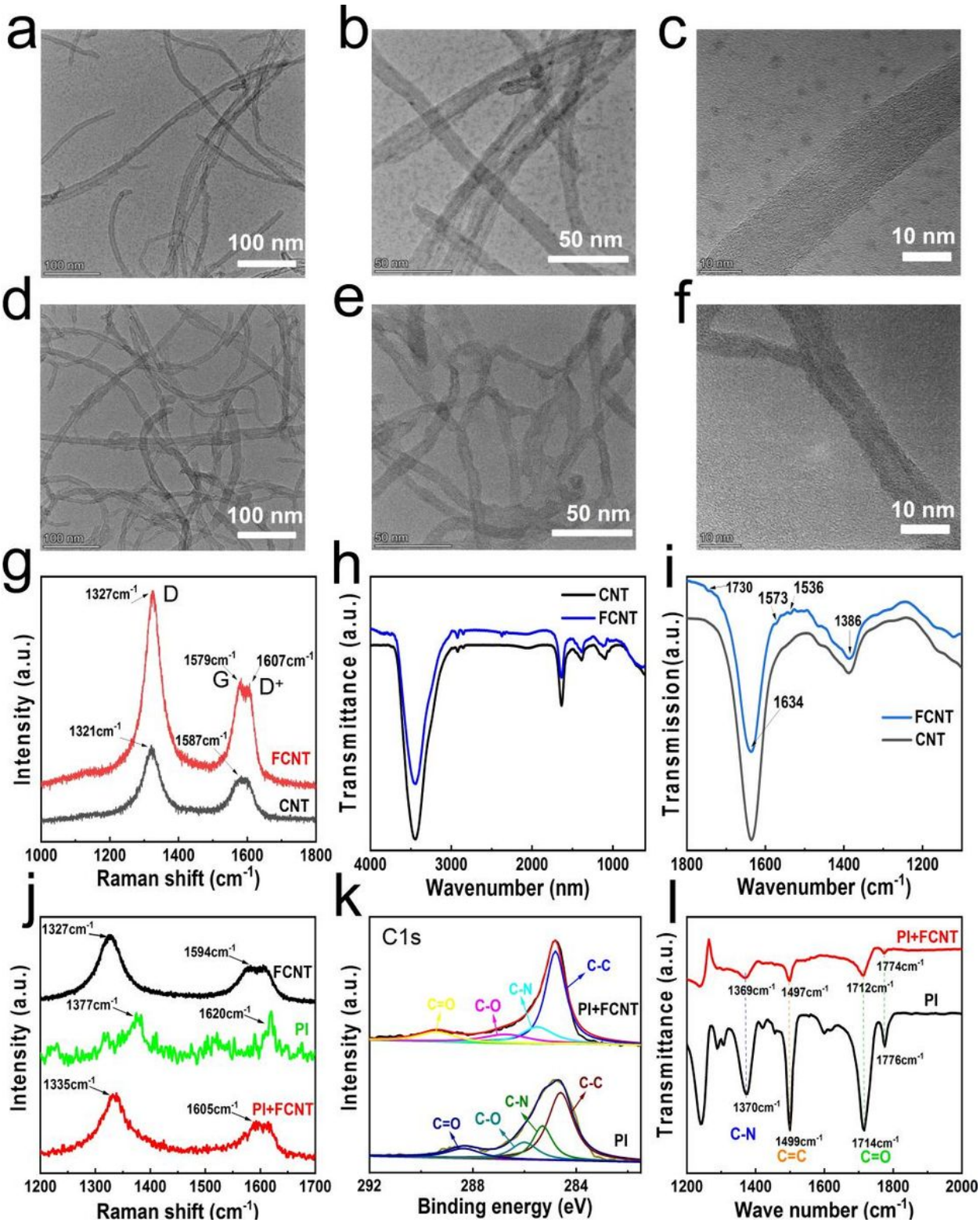

Figure 2

Characterization of CNT, FCNT, PI, and PI/FCNT(EPD). (a-c) TEM images of CNTs. (d-f) TEM images of FCNTs. (g) Representative Raman spectra of CNT and FCNT. (h-i) FT-IR spectra of CNT and FCNT. (j) Representative Raman spectra of PI, FCNT, and PI/FCNT(EPD). (k) XPS survey (C1s) spectra of PI and PI/FCNT(EPD). (l) FT-IR spectra of PI and PI/CNT (EPD).

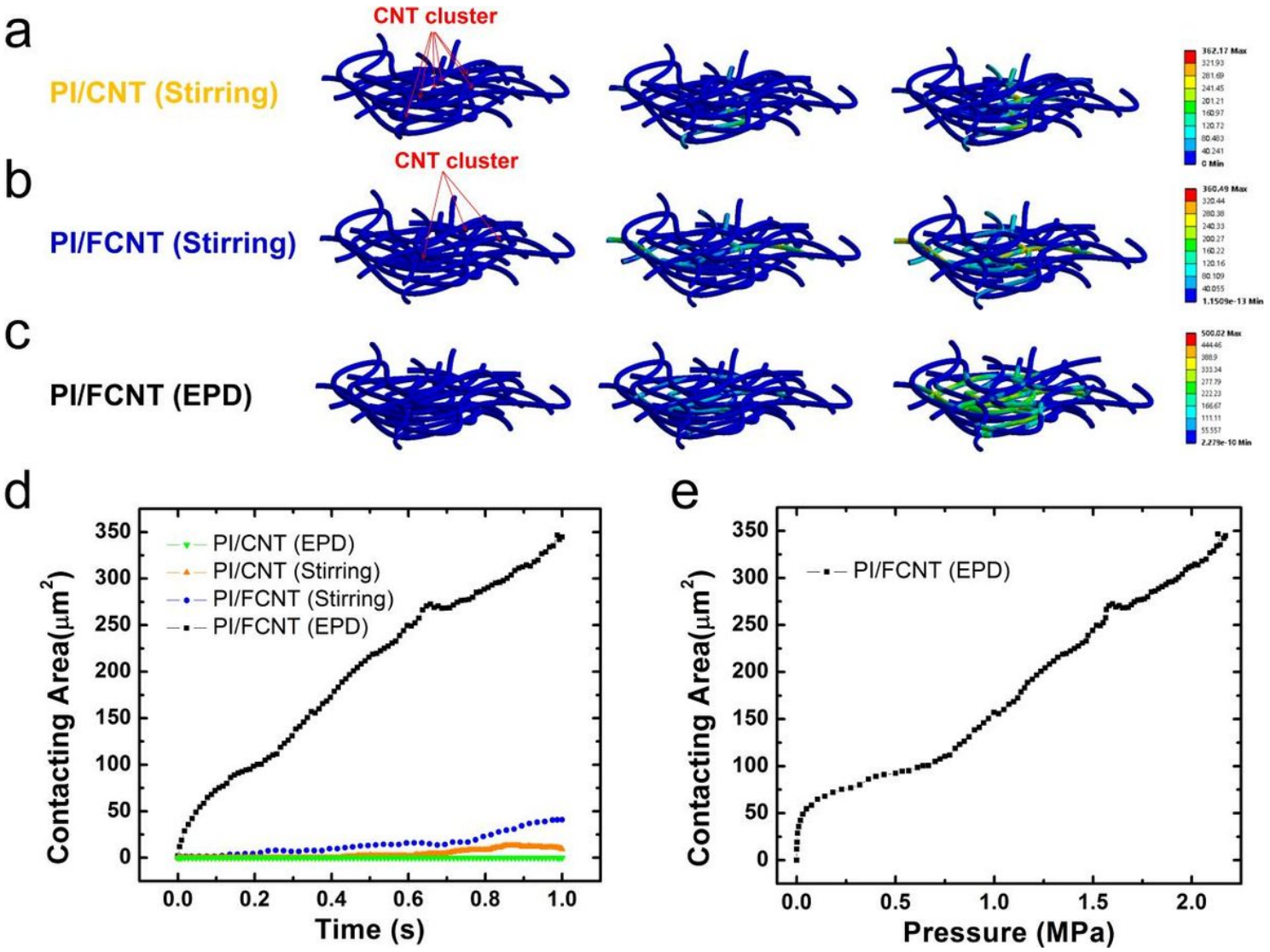

Figure 3

Finite element analysis of proposed pressure sensors. (a-c) Microscopic deformation process for the model with PI/CNT(Stirring), PI/FCNT(Stirring), and PI/FCNT(EPD), respectively. (d) Contacting area as a function of time for the proposed four sets of pressure sensors. (e) Contacting area vs. Pressure curve for PI/FCNT(EPD) pressure sensor.

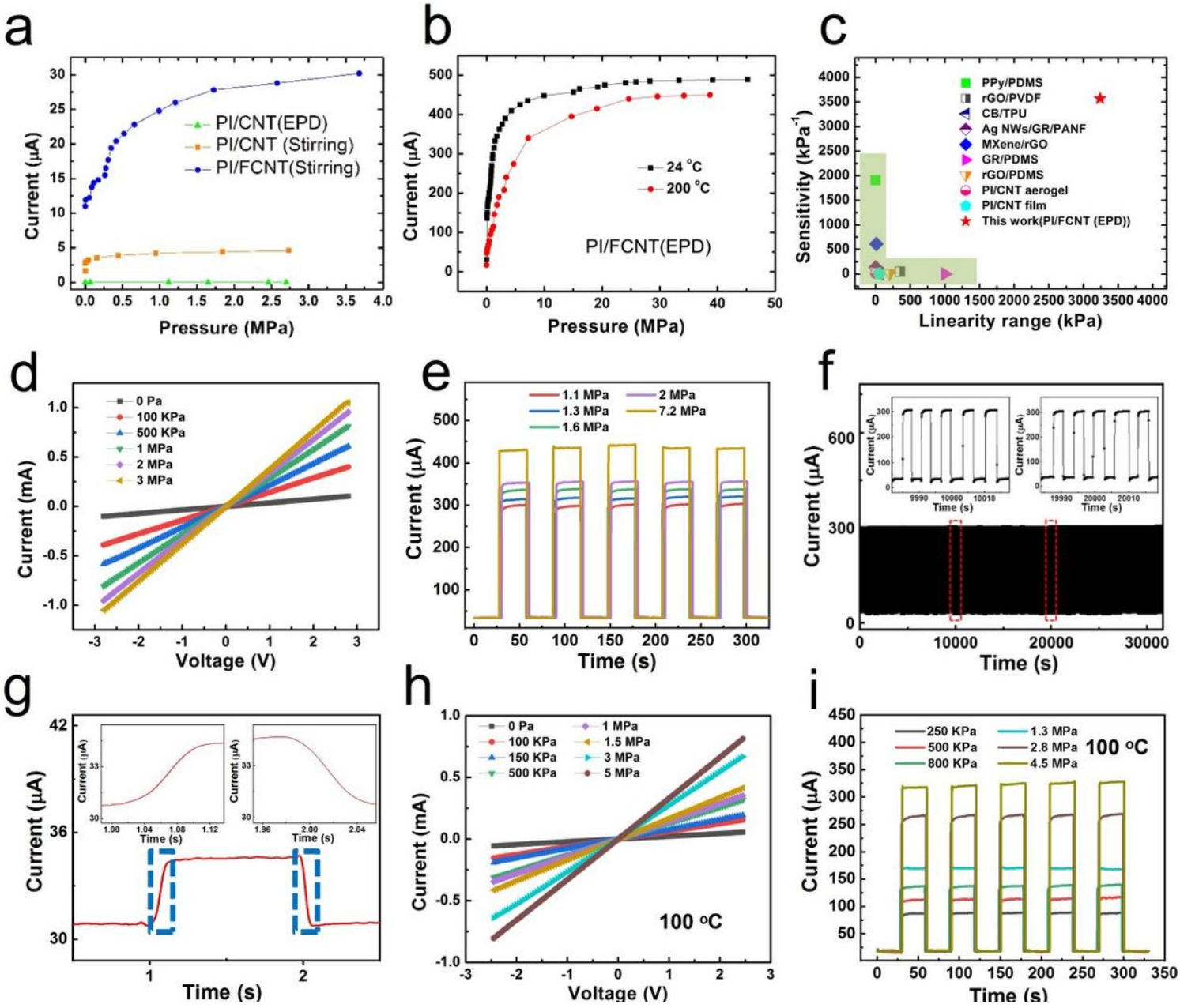

Figure 4

Pressure sensing performance of the fabricated pressure sensors. (a) Current response of the PI/CNT(EPD), PI/CNT(Stirring), and PI/FCNT(Stirring) pressure sensor. (b) Current response of the PI/FCNT(EPD) pressure sensor at room temperature and 200 °C. (c) Comparison of the sensitivity and linearity sensing performances based on this work and the previous reports. (d) I-V curves of the PI/FCNT(EPD) sensor device under different applied pressures. (e) Multiple cycles of pressure response under different pressures ranging from 1.1 MPa to 7.2 MPa. (f) The durability test for the PI/FCNT(EPD) pressure sensor. (g) Response and relaxation time of the PI/FCNT(EPD) pressure sensor. (h) I-V curves with different loading pressure ranging from 0 Pa to 5 MPa at 100 °C. (i) The relative current variation of the PI/FCNT(EPD) pressure sensor under repeated pressures ranging from 250 KPa to 4.5 MPa at 100 °C.

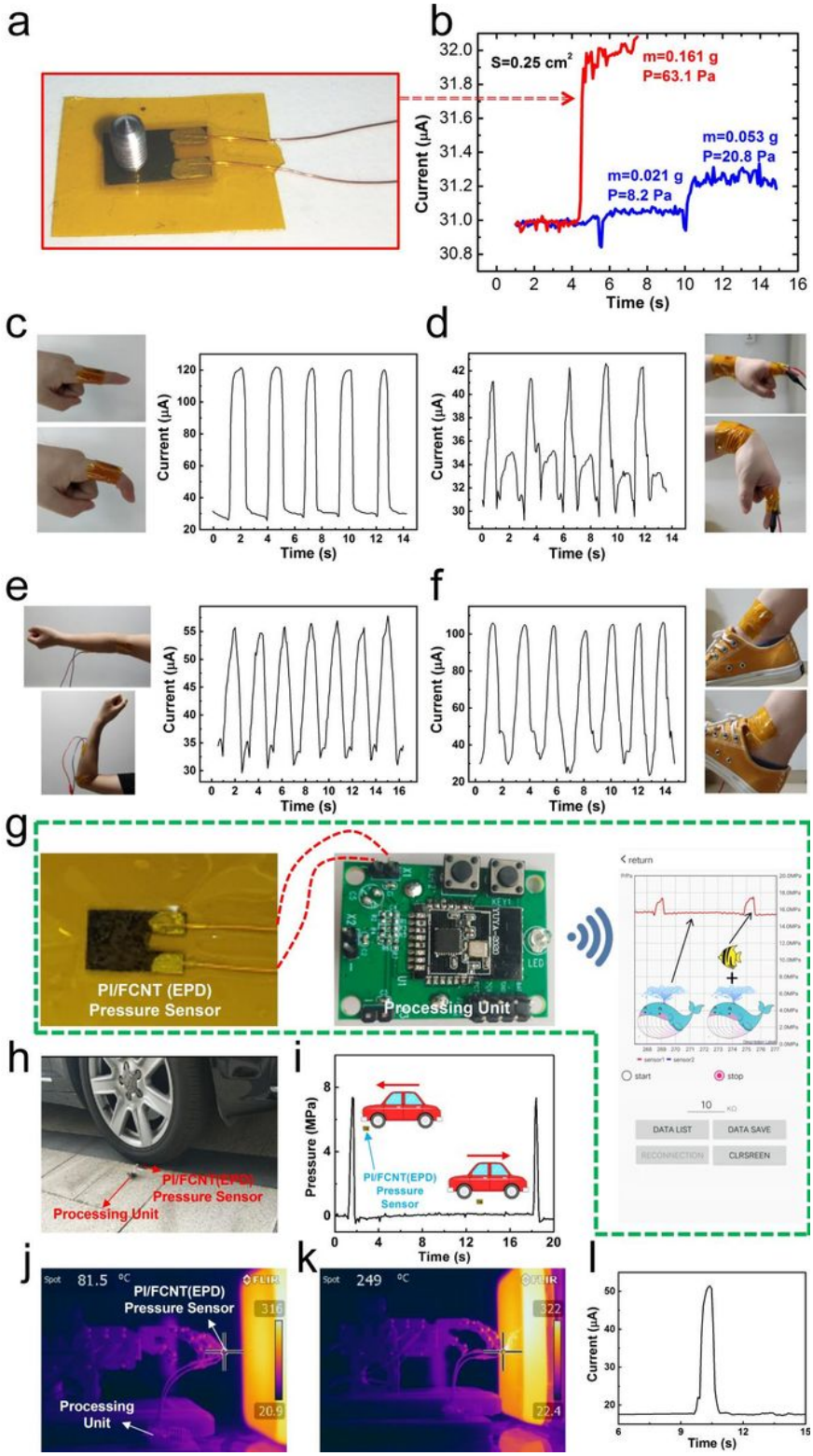

Figure 5

Application of the PI/FCNT(EPD) pressure sensor. (a-b) Detection of faint pressure: optical image and current curve of the proposed PI/FCNT(EPD) pressure sensor pressed by a small meter screw(0.161g, ~63.1 Pa); Current curves of the proposed PI/FCNT (EPD) pressure sensor pressed by aluminum particle with 0.021 g and 0.053 g (0.021 g+0.032 g), respectively. Faint pressures (~8.2 Pa) can be detected by the PI/FCNT(EPD) pressure sensors. (c-f) Detection of low pressure: monitoring of finger bending, wrist

movement, elbow bending, and ankle movement. (g) A wireless, real-time pressure monitoring system, including PI/FCNT(EPD) pressure sensor, processing unit, and mobile APP. Right of (g): detection of relatively low pressure under high pressure. (h, i) Detection of high pressure: Real-time pressure monitoring of the sensor device when subjected to high pressure applied by driving a car over the sensor device repeatedly. (j-l) Intelligent robots ‘feel’ the pressure under a high-temperature environment: IR images of the mechanical hand with the PI/FCNT(EPD) pressure sensor as the mechanical hand get close to and touches the hot object (j, k); Signal response of the intelligent robot (with the integrated proposed sensor as the perception layer) during the ‘close, touch, feel and response’ process.

Supplementary Files

This is a list of supplementary files associated with this preprint. Click to download.

- SupportingInformation.docx